International Journal of
Turbomachinery Propulsion and Power

MDPI

Article

3D Numerical Modeling of Zeotropic Mixtures and Pure Working Fluids in an ORC Turbo-Expander

Ibrahim Gad-el-Hak *, Ahmed E. Hussin, Ashraf M. Hamed and Nabil A. Mahmoud

Department of Mechanical Engineering, Ain Shams University, 11517 Cairo, Egypt;
ahmed_eldeinhussin@eng.asu.edu.eg (A.E.H.); ashraf.mostafa@eng.asu.edu.eg (A.M.H.);
Nabil_Mahmoud@eng.asu.edu.eg (N.A.M.)

* Correspondence: ibrahim_gad@eng.asu.edu.eg; Tel.: +20-111-366-6233

Academic Editor: Marcello Manna
Received: 26 December 2016; Accepted: 15 March 2017; Published: 21 March 2017

Abstract: The present paper provides a numerical study that leads to the proper selection of a working fluid for use in low-temperature organic Rankine cycle (ORC) applications. This selection is not only based on the provision of best efficiency but also to comply with global warming potential (GWP) regulations. For that purpose, different pure organic working fluids, including R245fa, R236fa, R123, R600a, R134a, and R1234yf as well as zeotropic mixture R245fa/R600a, are selected. The investigation is conducted on a single stage radial inflow turbo-expander, which was originally used in the Sundstrand Power Systems T-100 Multipurpose Small Power Unit. The commercial package ANSYS-CFX (version 16.0) was used to perform the numerical study using 3D Reynolds-Averaged Navier–Stokes (RANS) simulations. Peng–Robinson equation of state is adopted in the finite-volume solver ANSYS-CFX to determine the real-gas properties. The obtained results show that, while the use of R134a and R1234yf provides the best efficiency of all the working fluids under investigation, the latter is best selected for its comparatively low global warming effects.

Keywords: radial inflow turbine; organic Rankine cycles; working fluids; computational fluid dynamics; zeotropic mixtures

1. Introduction

Organic Rankine cycle (ORC) technology has been introduced as a means of waste heat recovery to reduce consumption of conventional energy resources, greenhouse gases and harness renewable energy sources [1]. However, the efficiency of ORC is about 10%–20% due to its low operating temperatures [2]. The performance of an ORC system correlates strongly with not only the selection of expansion machines, but also with the properties of the working fluids. Expanders used in the ORC system can be classified into two main types, namely (i) the volume type, such as scroll and screw expanders, and (ii) velocity type, such as radial inflow and axial flow turbines [3]. The choice of expander determines which working fluids can be employed in the ORC system [4].

Moreover, it was found that volumetric expanders have limitations due to its low built-in volume ratio, which does not match the required high volume ratios in ORC systems [4]. Another limitation is their swept volume, which limits the flow rate through the expander. Subsequently, running these expanders with low vapor density fluids is not recommended.

There are benefits to operating radial inflow turbines as expanders of an ORC due to (i) their lower sensitivity to blade profile inaccuracies than that of axial flow turbines, (ii) the high specific work per single stage, (iii) the lack of metal-to-metal contact as in scroll expanders, and (iv) the maintenance of high efficiency levels at off-design conditions, as demonstrated in [5].

Sauret and Rowlandset [6] performed a 1D meanline analysis of a radial inflow turbine with five different working fluids (R134a, R143a, R236fa, R245fa, and *n*-pentane). They found that R134a produced the best performance with a 33% increase in net power compared to *n*-pentane from the cycle operated at 150 °C.

The crucial factor in designing ORC turbines is that real (rather than ideal) gas properties must be used in modeling the expansion process [7]. Accordingly, the design process of a turbine operated with organic fluid has complexity, as opposed to that with air. Wong and Krumdieck [8] suggested switching an existing turbo-expander working with air to work with organic fluids in order to overcome the complexity of the design process for ORC turbo-expanders.

In addition, they introduced three approaches from dynamic similarity concepts to predict the performance curves for R245fa and R134a instead of air. However, the variable pressure ratio approach accurately predicted the optimal blade speed ratio, the maximum efficiency, and the mass flow rate, while a deviation was observed in predicting the best efficiency point.

The properties of the chosen working fluids have a significant influence on the performance of the ORC cycle. The following characteristics should be considered in selecting such working fluid as demonstrated in [9–11]:

- A high molecular weight;
- An acceptable evaporating pressure value to reduce both complexity and cost of evaporates;
- A high vapor density to avoid a large volume flow rate, consequently limiting the size of turbines, condensers, and evaporates;
- A positive slope or isentropic saturation vapor curve to prevent the formation of droplets at expansion process in a turbine and therefore avoiding pitting, corrosion, and erosion in turbine blades;
- A positive condensing gauge pressure in order to avoid air leakage into the cycle; and
- Low ozone depleting potential (ODP) and low global warming potential (GWP).

Much literature has been conducted on the working fluids selection [12–14] by comparison between a set of candidate working fluids from the thermodynamic analysis of a cycle and an assumed constant isentropic efficiency for a turbine. The performance of a radial inflow turbine has a relevant connection to fluid dynamic losses [15], which can be investigated by applying three-dimensional computational fluid dynamics (3D CFD) simulations.

Lopez Sanz [7] proved that organic working fluids should be considered real gases to predict accurate simulations. Thereby, the thermodynamic properties of a real gas need to be determined and linked with a CFD solver to attain accurate numerical results. Aghahosseini and Dincer [16] performed a comprehensive thermodynamics analysis of ORC with different pure/zeotropic working fluids. They found that refrigerant R123 produced lower irreversibility in the cycle. Moreover, Masheiti et al. [17] evaluated the performance of two working fluids, namely, R245fa and R134a, in a low-temperature geothermal ORC at 74 °C. They concluded that R245fa had a better performance due to the higher pinch temperature difference in the evaporator.

Zeotropic mixtures for working fluids have a significant effect on the performance of ORCs. Li et al. [18] examined the effect of various mixtures of working fluids with variable compositions on ORC performance. They found that a mixture of R245fa/R600a with composition (0.85/0.15) by weight has a potential effect on the net power output from an ORC.

The current paper screens for suitable organic fluids that work efficiently in low-temperature ORCs by providing three-dimensional numerical modeling of a radial-inflow turbine operated with various pure working fluids (R134a, R600a, R236fa, R245fa, R123, and R1234yf) and zeotropic mixtures (R245fa/R600a). Moreover, off-design conditions are discussed.

2. Working Fluid Selection and Design Parameters

The selection of these working fluids is a crucial step towards system performance. This selection should be based on thermodynamics properties as well as safety and environmental considerations. Here, the candidate working fluids have almost zero ozone depleting potential (ODP) and low global warming potential (GWP) in terms of reducing environmental impact. The selected pure organic working fluids for the current research were R245fa, R236fa, R123, R134a, R600a, and R1234yf. Furthermore, zeotropic mixtures between R245fa and R600a with variable compositions were examined. Table 1 provides physical properties, safety, and environmental data of the candidate working fluids.

Table 1. Physical properties, safety, and environmental data of the candidate working fluids [14].

Working Fluids	Physical Properties				ASHRAE Safety Group	Environmental Data		
	Slope	Critical temperature (K)	Critical pressure (kPa)	Molecular weight (kg/kmol)		ODP	GWP (100 Years)	Atmospheric Life Time (Year)
R245fa	Positive	447.4	3.93	134.05	A1	0	950	7.6
R236fa	Positive	398.07	3.2	152.04	A1	0	9810	242
R123	Positive	456.7	3.66	152.93	B1	0.02	77	1.3
R600a	Positive	408	3.64	58.122	A3	0	8	1
R134a	Wet	374	4.06	102.03	A1	0	1430	14
R1234yf	Positive	367.85	3.38	114.04	A2L	0	<1	0.029

ODP, ozone depleting potential; GWP, global warming potential.

There are several recommended optimal boundaries that should be fulfilled in order to operate radial turbines efficiently in the cycle [4]:

(a) The specific speed $\Omega_S = \left(\frac{\omega\sqrt{Q}}{(\Delta h_{is})^{3/4}}\right)$ should lie between 0.5 and 0.9 (see Figure 1, Dixon and Hall [19]).

(b) The upper limit of the tip speed must be within 370 m/s [4].

(c) A maximum relative Mach number $\left(M_3 = \frac{W_3}{a_3} = 0.85\right)$ is generally recommended in order to avoid a choked flow in the rotor.

(d) The upper limit of the absolute Mach number at the nozzle exit should not exceed 1.8 [4].

(e) The maximum efficiency occurs in the ranges of (see Figure 2, Chen and Baines [20])

- 0.2–0.3 for the flow coefficient $\left(\Phi = \frac{C_{m3}}{U_2}\right)$ and
- 0.7–0.9 for loading coefficient $\left(\Psi = \frac{\Delta h_o}{U_2{}^2}\right)$.

(f) The tip Mach number $\left(M_U = \frac{U_2}{a_2}\right)$ lies in the range 0.5–0.7 for automotive turbocharger turbines, while the value of tip Mach number is increased to 1, and choking must be considered for low-temperature turbines (refrigerant expander) (see Cox [21]).

(g) The blade speed ratio ($\frac{U_2}{C_0}$) should be close to 0.7 for most efficient turbines, where C_0, the spouting velocity, is the velocity of a jet if the gas was expanded isentropically through a nozzle, and equals $\sqrt{2\Delta h_{is}}$ (see Cox [21]).

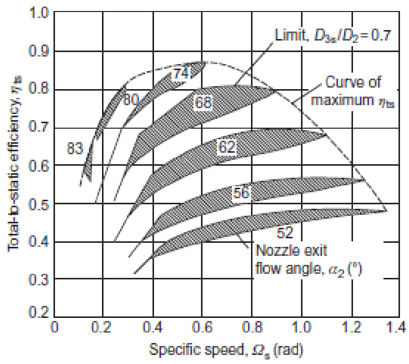

Figure 1. Efficiency curve of a radial inflow turbine as a function of its specific speed. Reproduced from [19], Copyright 2013, with permission from Elsevier.

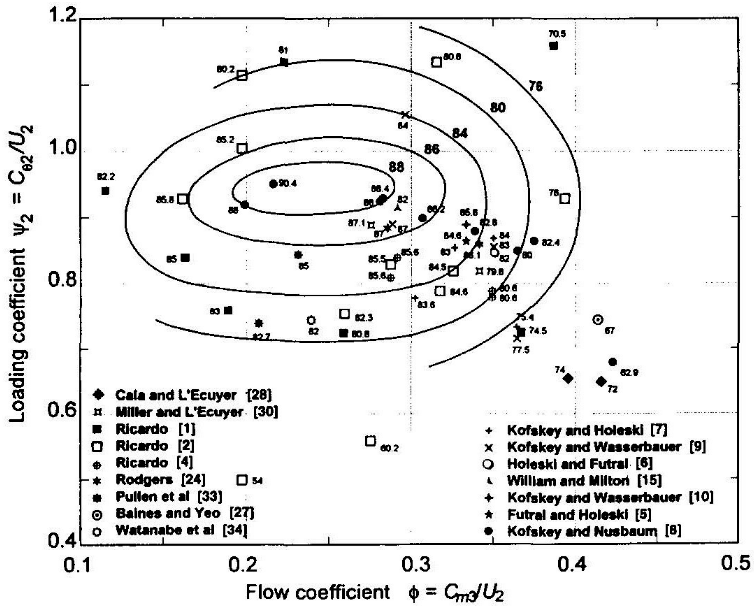

Figure 2. Correlation of measured efficiency of a range of radial inflow turbine designs with stage loading and flow coefficient. Reproduced from [20], Copyright 1994, with permission from Elsevier.

3. Numerical Method

Three-dimensional numerical modeling was performed on the radial inflow turbine geometry to examine the effect of the candidate working fluids on the performance using a commercial package-finite volume solver ANSYS-CFX (version 16.0, ANSYS Inc., Cannonsburg, PA, USA).

3.1. Computational Domain

A single stage radial inflow turbine, which is normally used in the Sundstrand Power Systems T-100 Multipurpose Small Power Unit [22], was selected as the baseline geometry to carry out the numerical modeling. The geometry of this turbine is published in [23]. The distribution of wrap angle, blade angle, and blade thickness are imported in ANSYS Blade-Gen (version 16.0, ANSYS Inc.) to generate a solid model for the rotor and the nozzle blades as shown in Figure 3. Figure 4 presents the full details of the radial inflow turbine geometry. The turbine consists of 19 nozzle blades and 16 rotor blades.

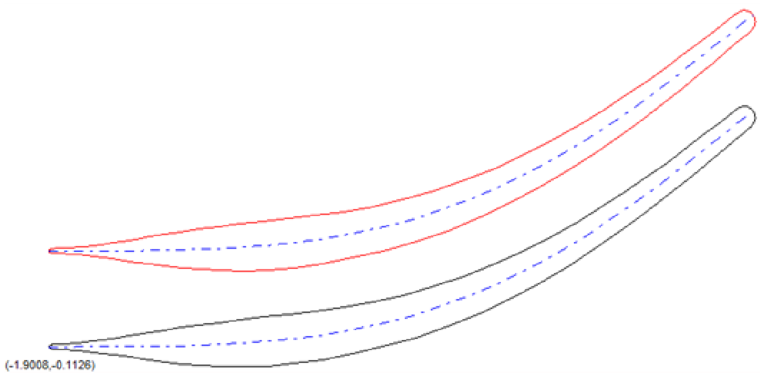

(**a**)

Figure 3. *Cont.*

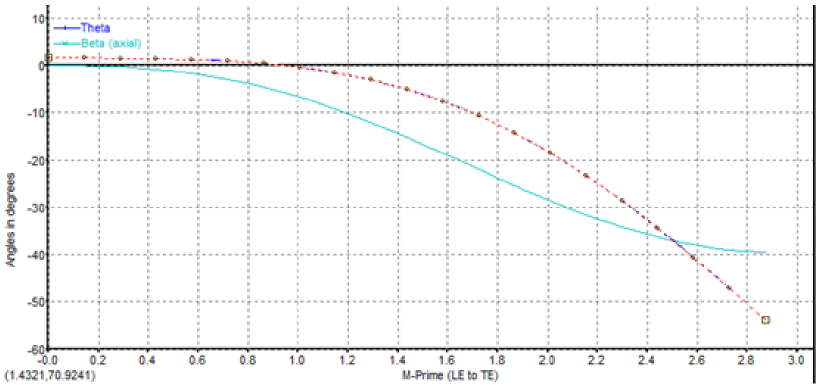

(**b**)

Figure 3. Blade to blade view (**a**) and the distribution of wrap angle and blade angle (**b**) at the hub of the rotor blades.

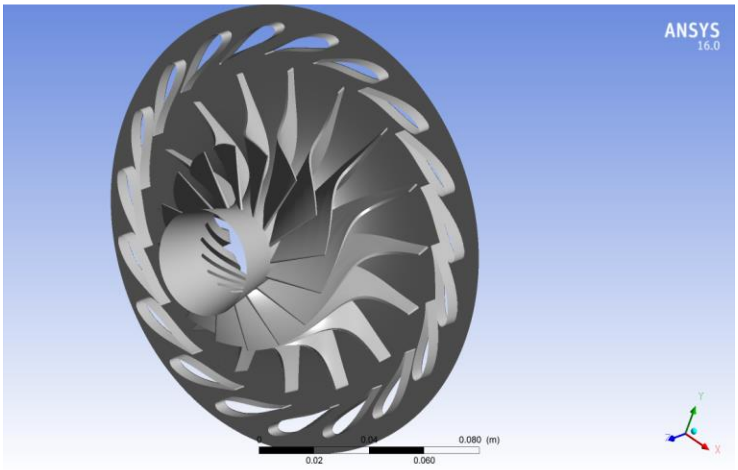

Figure 4. Geometry of the radial inflow turbine.

3.2. Boundary Conditions

To validate the numerical results with the experimental data that were conducted by Jones [22], the following set of boundary conditions are defined:

a) The total temperature of 477.6 K and the total pressure of 413.6 kPa were defined at the turbine inlet.
b) The outlet static pressure was 72.4 kPa to produce a pressure ratio (*t-s*) equal to 5.73.
c) The working fluid that was used in the experimental data of [22] was air and was assumed as an ideal gas in the CFD simulations.
d) The nominal rotational speed for the turbine was set to 71,700 rpm, equal to that of the experimental data [22].

In this study, two mixing models, frozen rotor and stage model were tested at the interface between rotor and stator. The frozen rotor model was selected against the stage model because it agrees well with experimental data [22] with a 1% maximum deviation.

A single blade passage model including the stator, the rotor, and part of the diffuser was selected to perform the flow simulation over the full turbine to reduce computational time [24]. The periodic boundaries were specified at both sides of the stator and the rotor passage, as shown in Figure 5.

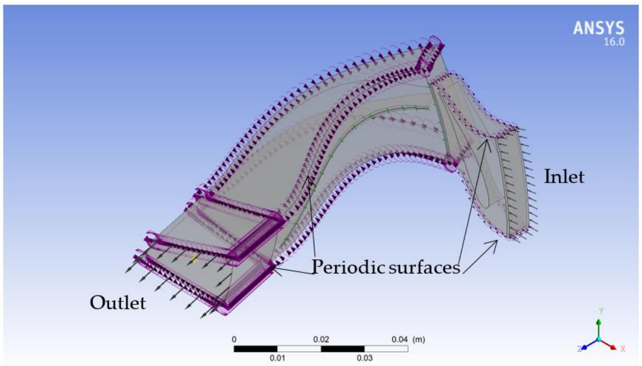

Figure 5. Boundary conditions for a single blade passage including the rotor, the stator, and part of the diffuser.

3.3. Mesh

ANSYS Turbo-Grid was used to generate a structured grid (hexahedron) for the flow passage for both the rotor and the stator. Automatic topology and meshing (ATM Optimized) was applied to the stator and the rotor flow passages to fit a proper topology for the blade passage. The method "proportional to mesh size" was chosen in the boundary layer refinement control with a setting factor base and factor ratio of 0 and 1.6 respectively, which is recommended in [25].

A mesh independency test was performed by running the simulation case from a very coarse mesh (with 203,008 elements) to a very fine mesh (with 2,280,541 elements). The numerical calculations may be regarded to be grid-independent with 1,965,103 elements, including the rotor and the stator, as presented in Figure 6. The recommended value of non-dimensional grid spacing (y^+) at the wall is 1.0 for the k–ω turbulence model; however, the typical value of y^+ at the rotor blade was 6.49. Therefore, the option of automatic wall functions was selected, which allows the k–ω model to obtain good predictions even if the value of y^+ is larger than 1.0. All simulations cases were performed until residuals dropped to 10^{-6}. Figures 7 and 8 present the converged grid for the nozzle blade and the rotor blade, respectively, at 1,965,103 elements.

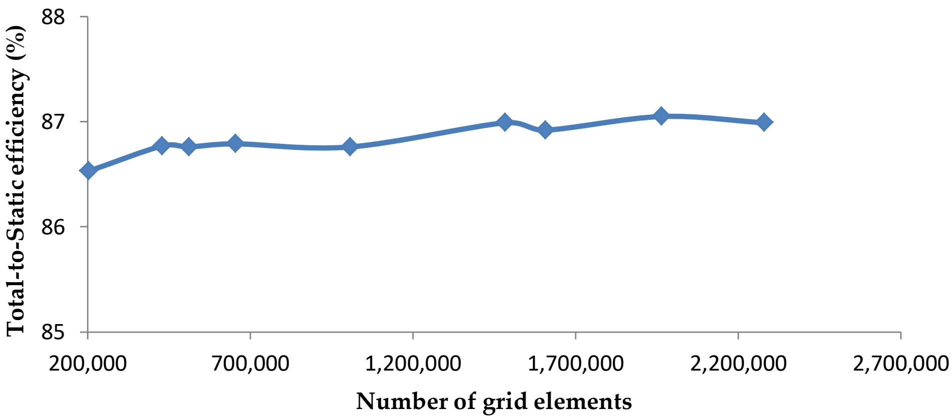

Figure 6. Grid independency test.

The following parameters were used to check the quality of the grid:

a) Face angle: the angle between the edges of each face within an element. The final mesh analysis of rotor flow passages shows 23.27° for minimum face angle and 156.72° for maximum face angle.
b) Minimum Volume: the minimum volume of each cell. Its value is 1.922×10^{-15} m^3.
c) Connectivity Number: the number of elements connected to a single node. Its value is 10.

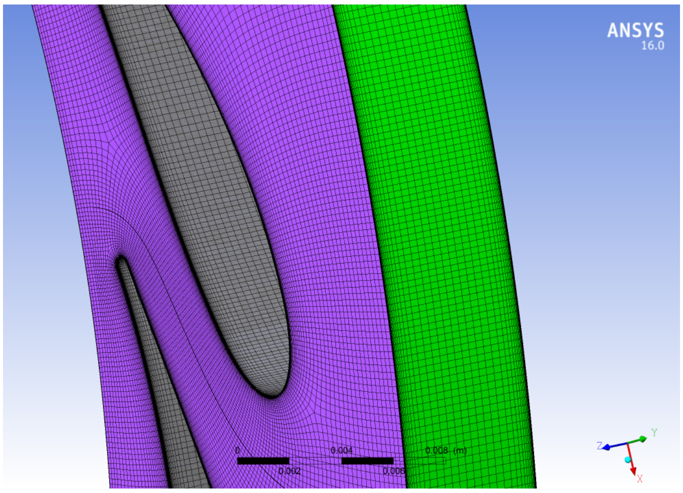

Figure 7. 3D computational grids at the nozzle blade with a grid density of 829,180.

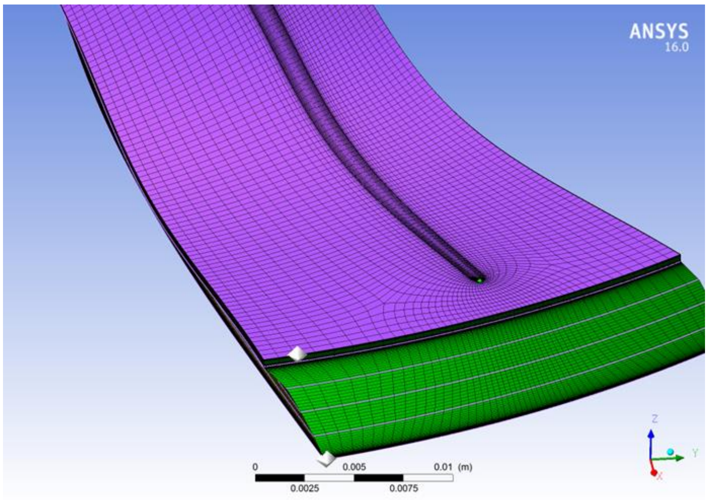

(**a**)

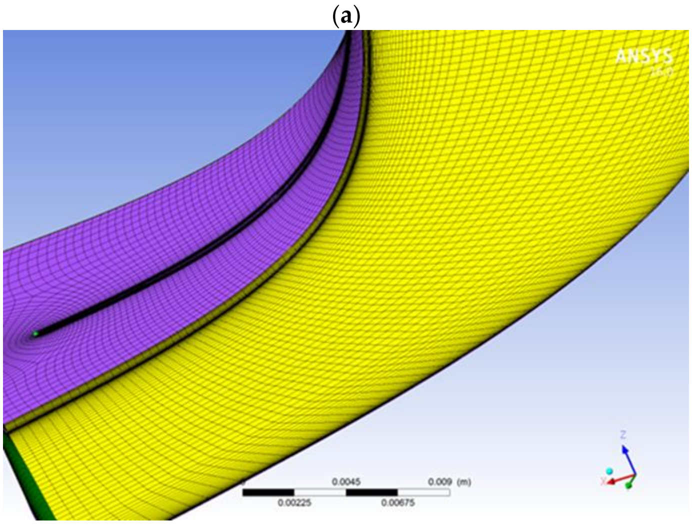

(**b**)

Figure 8. 3D computational grids at the front view (**a**) and the side view (**b**) of the rotor with grid density of 1,135,923 elements.

3.4. Numerical Details

Commercial package ANSYS-CFX (version 16.0) was selected to perform the finite volume, steady state, three-dimensional Navier–Stokes (RANS) approach for flow simulations. A high-resolution scheme was used to solve governing equations. Two turbulence models, k–ε and k-ω, were tested. The k-ω turbulence model with an automatic wall function was found to be the most comparable to the experimental data.

As mentioned earlier, the properties of organic fluids must be determined and employed in a finite volume solver. The Peng–Robinson equation of state [26] was implemented to provide reasonable accuracy in predicting real gas properties [27]. Equation (1) describes the Peng–Robinson equation of state.

$$p = \frac{RT}{V_m - b} - \frac{a\alpha}{{V_m}^2 + 2bV_m - b^2} \tag{1}$$

Where;

$$a = \frac{0.457235R^2\ {T_c}^2}{p_c}$$

$$b = \frac{0.077796RT_c}{p_c}$$

$$\alpha = \left(1 + k\left(1 - {T_r}^{0.5}\right)\right)^2$$

$$T_r = \frac{T}{T_c}$$

$$k = 0.37464 + 1.54226\omega - 0.26992\omega^2$$

where ω is the acentric factor of the working fluid, p_c and T_c are the critical pressure and temperature, respectively, of the working fluid. R is the universal gas constant, and V_m is the molar volume.

4. Numerical Results and Discussion

4.1. Validation of the Numerical Results

Two types of efficiency can be calculated in order to investigate the performance of the turbine: the total-to-static and total-to-total isentropic efficiencies, as described in Equations (2) and (3), respectively. The values of the total-to-static efficiency from 3D CFD RANS simulations at different blade speed ratios were compared with the experimental data available in [22]. The comparison is presented in Figure 9. The obtained numerical results have good agreement with that of the experiments, with a maximum deviation <1%. However, the predicted peak efficiency occurs at a blade speed ratio of 0.72, which is slightly shifted from that of the experimental data.

$$\eta_{t-s} = \frac{h_{01} - h_{03}}{h_{0_1} - h_{S_{is\ 3}}} \tag{2}$$

$$\eta_{t-t} = \frac{h_{01} - h_{03}}{h_{0_1} - h_{0_{is\ 3}}} \tag{3}$$

At the nominal blade speed ratio (U_2/C_0 = 0.7), the flow remained obviously attached to the suction surfaces of the rotor blades. However, at higher blade speed ratios (greater than 0.7), the flow streamlines got separated from these suction surfaces of the rotor blades, leading to the generation of a secondary flow and hence flow separation. This is reflected in the reduction in efficiency (Figure 9). Figures 10 and 11 show the blade loading and streamlines of velocity around the blade at four blade speed ratios: 0.56, 0.7, 0.77, and 0.805.

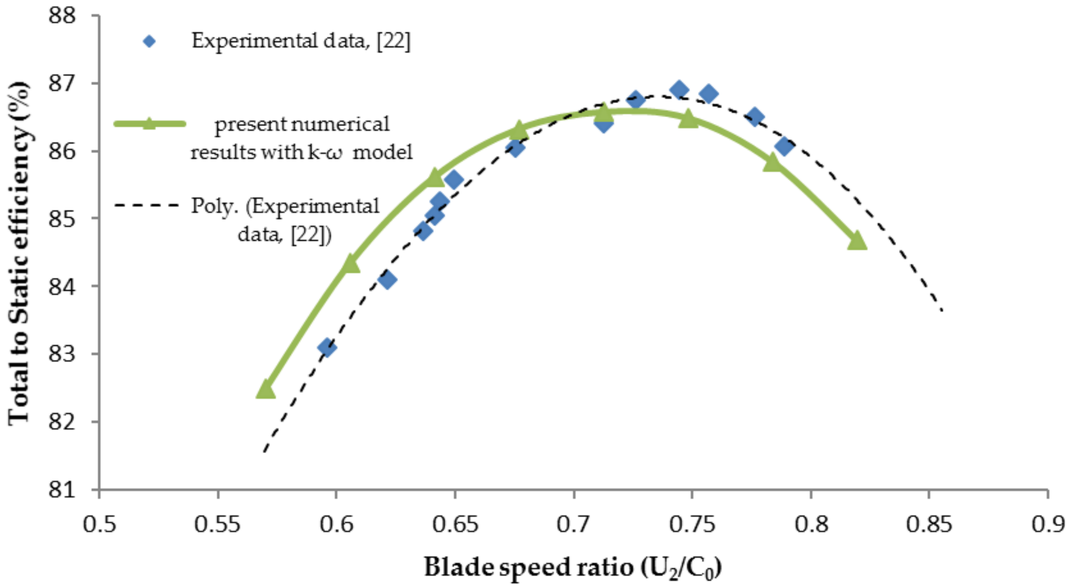

Figure 9. Validation of total-to-static efficiency from computational fluid dynamics (CFD) simulations with experimental data [22].

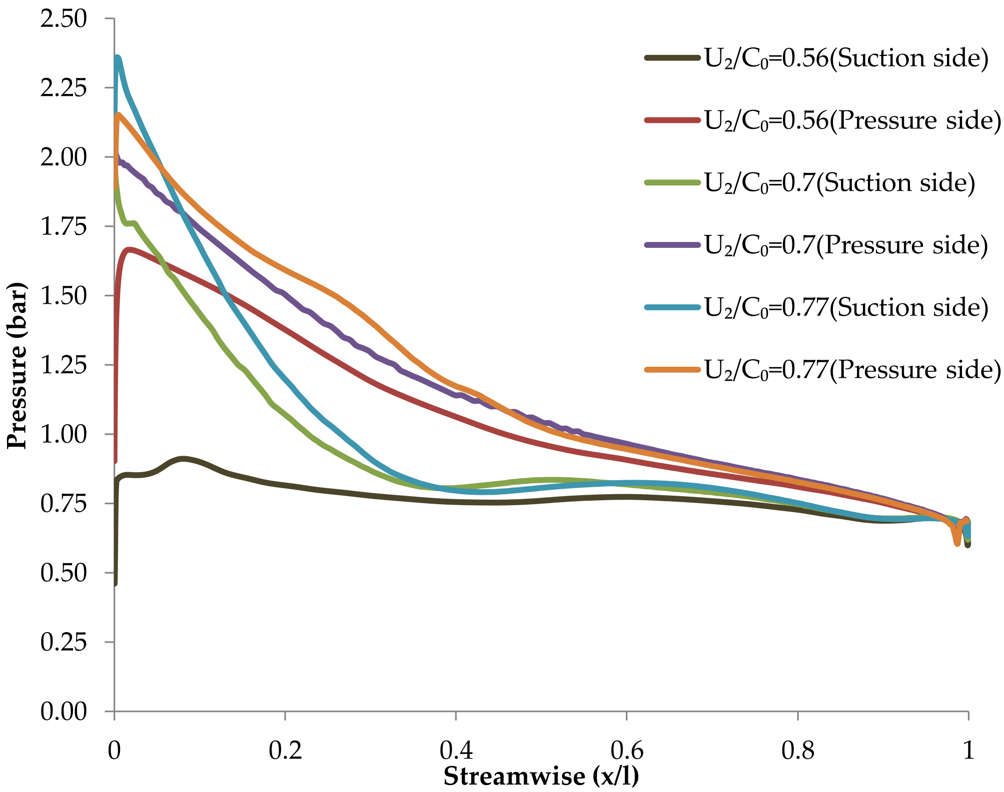

Figure 10. Blade loading for three different blade to spouting velocity ratio at 50% span.

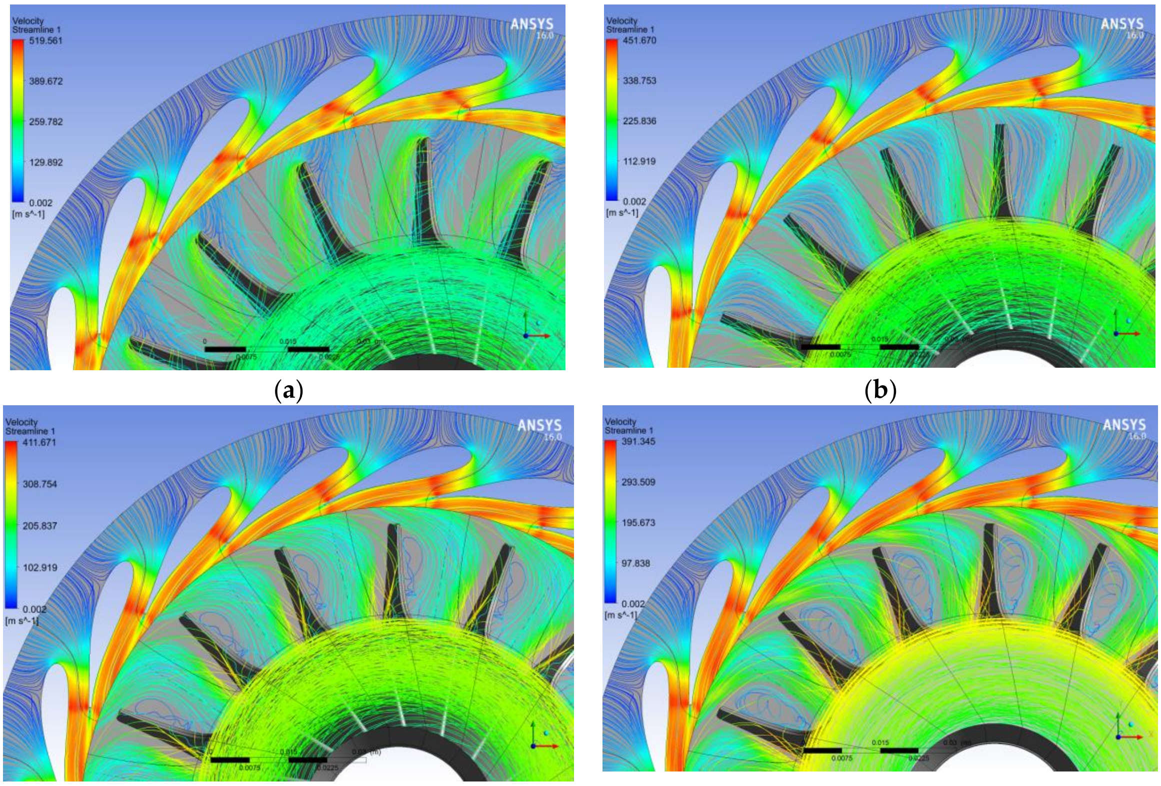

(**a**) (**b**)

(**c**) (**d**)

Figure 11. 3D velocity streamlines for four different blade to spouting velocity ratio U_2/C_0 = 0.56 (**a**), U_2/C_0 = 0.7 (**b**), U_2/C_0 = 0.77 (**c**), and U_2/C_0 = 0.805 (**d**).

4.2. Numerical Results of Pure Working Fluids

In this analysis, simulations were performed to investigate the optimal working fluid in turbo-expander for ORC powered by low grade energy. The inlet and outlet turbine temperatures were fixed to 370 K and 313 K, which is 10 K higher than that of the ambient temperature for all simulations. According to Hung [28], the working fluid had to be supplied to the turbine in a saturated vapor condition to reduce the irreversibility of the cycle. Therefore, the inlet turbine pressure was defined corresponding to the saturated vapor pressure at T = 370 K for each working fluid, while the outlet turbine pressure was defined by assuming an isentropic expansion process. REFPROP Version 9.0 [29] was used to estimate the properties of pure fluids and zeotropic mixtures between R245fa and R600a. R134a is a wet type refrigerant; thereby, the inlet pressure was adjusted by modeling the isentropic expansion process as a saturated vapor at outlet condition to a pressure corresponding to T = 370 K, which lies in the superheated region. The rotational speed was selected to maintain the same blade speed ratio (U_2/C_0 = 0.7) for each working fluid. Table 2 shows the operating conditions for the candidate working fluids.

Table 2. Operating conditions for the candidate selected working fluids.

Working Fluid	Inlet turbine pressure (kPa)	Inlet turbine temperature (K)	Outlet turbine pressure (kPa)	Outlet turbine temperature (K)	Pressure ratio (*Pr*)	Rotational turbine speed (RPM)
R245fa	1178	370	166	313	7.10	31098
R236fa	1814	370	286	313	6.34	27193
R123	731	370	111	313	6.59	29076
R600a	1872	370	395	313	4.74	40219
R134a	3234	370	1012	313	3.20	24403
R1234yf	3242	370	999	313	3.25	22258

Figure 12 shows the variations of total-to-static efficiency ($\eta_{t\text{–}s}$) and total-to-total ($\eta_{t\text{–}t}$) with blade speed ratios (U_2/C_0) for each working fluid.

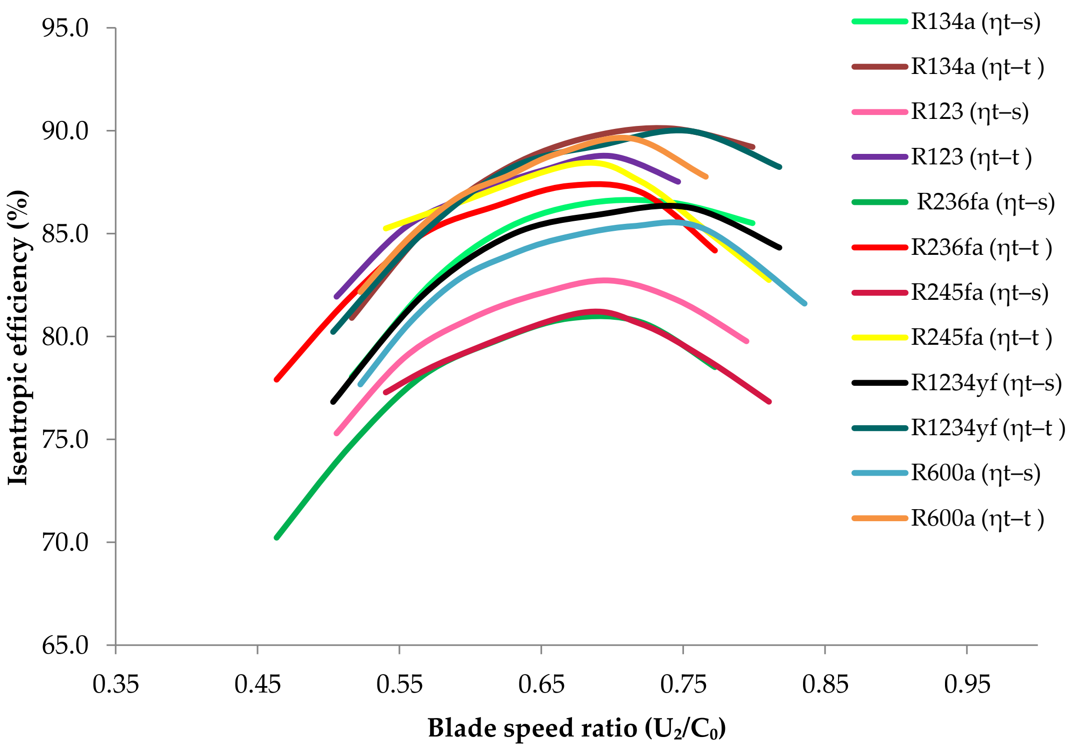

Figure 12. Comparisons of total-to-static and total-to-total efficiency for each working fluid with blade speed ratios.

The figure shows that the working fluids (R134a and R1234yf) produce higher total-to-static turbine efficiency due to lower pressure ratios across the turbine: 2.20 and 2.25, respectively. The lowest efficiency (81%) was obtained using the working fluids R236fa and R245fa at U_2/C_0 = 0.7 with corresponding pressure ratios of 6.34 and 7.10, respectively. This high pressure ratio leads to a highly choked flow condition in both the nozzle and the rotor, which leads to greater energy losses and thereby lowers the overall turbine efficiency.

Figure 13 presents a relative Mach number distribution at mid-span. It can be observed that the choked flow occurred in the nozzle for all working fluids with a maxmium Mach number of approximately 1.3 for Refigerants R236fa, R600a, R1234yf, and R123, while its value for R245fa and R134a was slightly lower than the other refigrants with a maxmium value of 1.25.

However, the exit flow from the rotor was a subsonic flow for refigerants R1234yf, R600a, and R134a with maxmium Mach numbers of 0.6, 0.84, and 0.6 respectively, while choked flow occurred at the exit of the rotor for refigerants R245fa, R236fa, and R123 with maximum Mach numbers of 1.34, 1.18, and 1.2 respectively due to high pressure ratios across the turbine. Consequently, the radial inflow turbine is not suitable to operate at high pressure ratios in ORC systems to avoid choked flow at rotor exit for refigerants R245fa, R236fa, and R123.

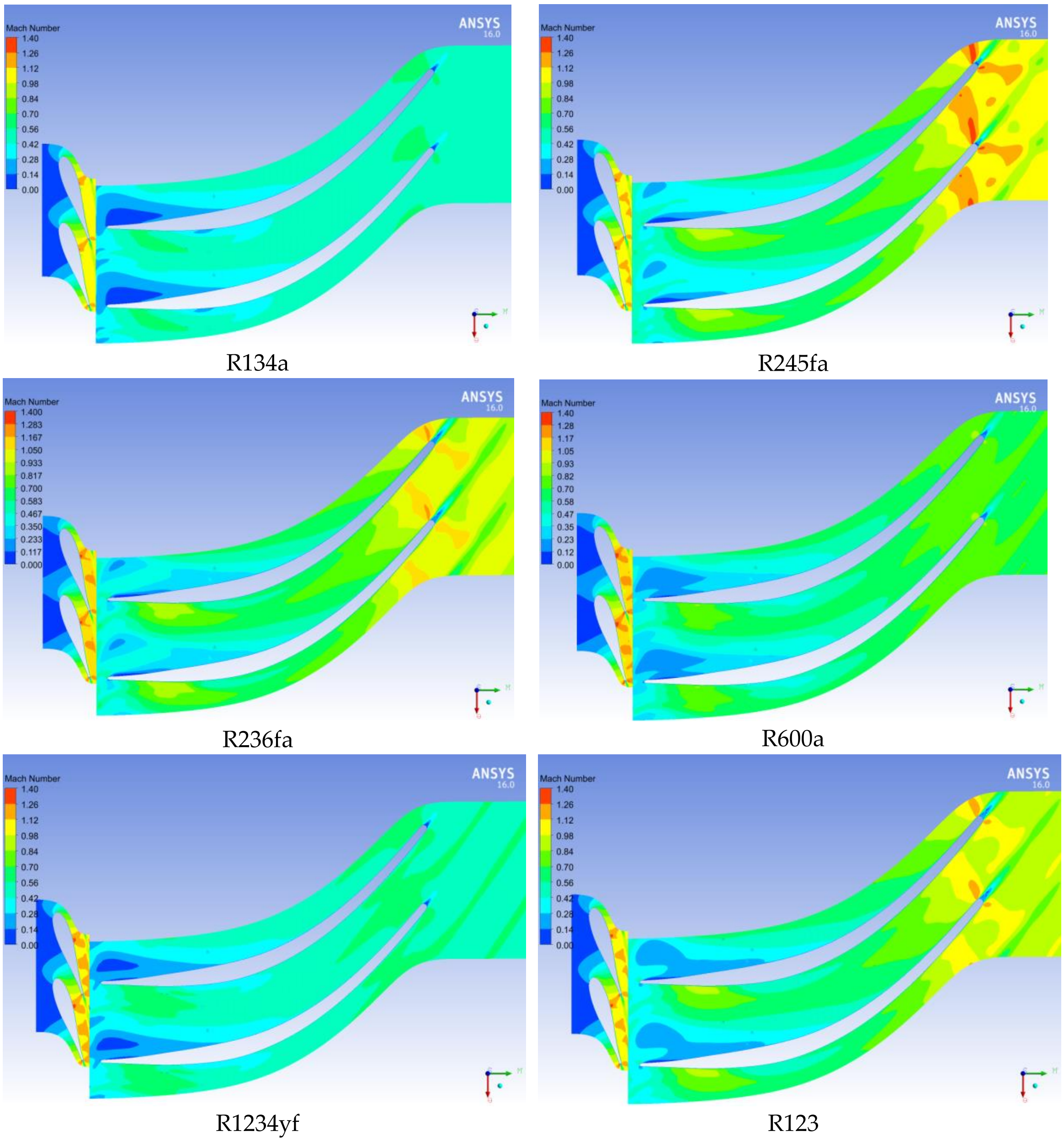

Figure 13. Relative Mach number contours around the stator and the rotor at mid-span for the selected working fluids at U_2/C_0 = 0.7.

In order to check the validity of a radial-inflow turbine to act as an expander in low-temperature ORCs with different organic working fluids, the specific speed parameter (Ω_S), the flow coefficient (φ), and the stage loading coefficient (Ψ) were used. The specific speed (Ω_S) defined by Equation (4) as shown by Dixon [19] is plotted with a total-to-static efficiency at different working fluids in Figure 14. As previously mentioned, the recommended range of the specific speed is between 0.45 and 0.8.

$$\Omega_S = \frac{\omega\sqrt{Q}}{(\Delta h_{is})^{3/4}} \tag{4}$$

where Q is the volumetric flow rate in m^3/s at the rotor outlet, and Δh_{is} (J/kg) is the isentropic enthalpy drop from stage inlet total conditions to the rotor exit static pressure.

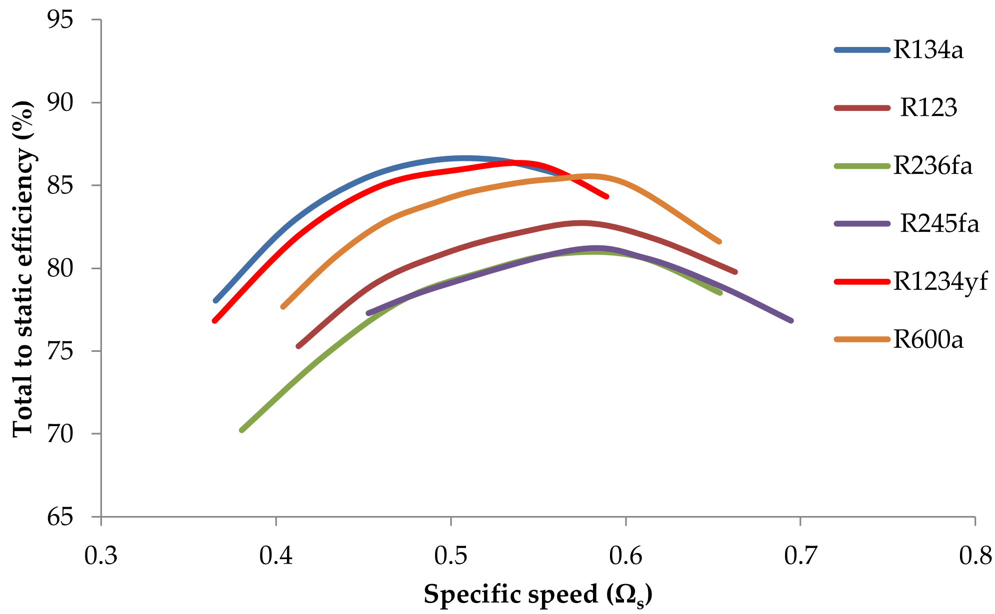

Figure 14. Total-to-static efficiency for each working fluid with specific speeds at off design conditions.

Figure 14 indicates that the calculated specific speeds for different working fluids lie within the recommended range, indicating that the radial turbine is suitable for these particular operating conditions. Thereby, the selected rotational turbine speed based on maintaining the same blade speed ratio (U_2/C_0) with different working fluids is an appropriate choice for scaling a radial inflow turbine from air as the working fluid to organic working fluids.

The flow coefficient (Φ) defined by Equation (5) is plotted versus efficiency in Figure 15.

$$\Phi = \frac{C_{m_3}}{U_2} \tag{5}$$

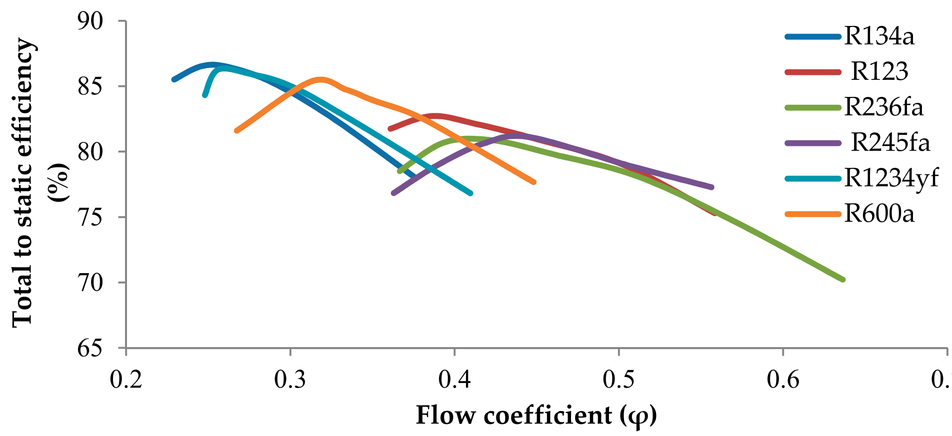

Figure 15. Flow coefficient for the selected working fluids with total-to-static efficiency.

The calculated flow coefficients indicate that the working fluids (R245fa and R236fa) have lower efficiency because their flow coefficients lie away from the optimum range, as shown in Figure 15. Thereby, the optimum range for flow coefficient mentioned by Baines and Chen [20] is valid for designing a radial inflow turbine in ORCs.

Another parameter correlating strongly with efficiency is the blade loading coefficient (Ψ) defined by Equation (6), which represents the work capacity of a turbine stage.

$$\Psi = \frac{\Delta h_o}{{U_2}^2}. \tag{6}$$

It can be seen from Figure 16 that the maximum efficiency points for all working fluids are matched with the recommended range for blade loading coefficient from 0.7 to 0.9; however, R1234yf and R134a have a higher total-to-static efficiency than the other working fluids for the same range of blade loading coefficients. Therefore, both the blade loading coefficient and the flow coefficient must be carefully considered together in order to estimate the efficiency of a radial inflow turbine.

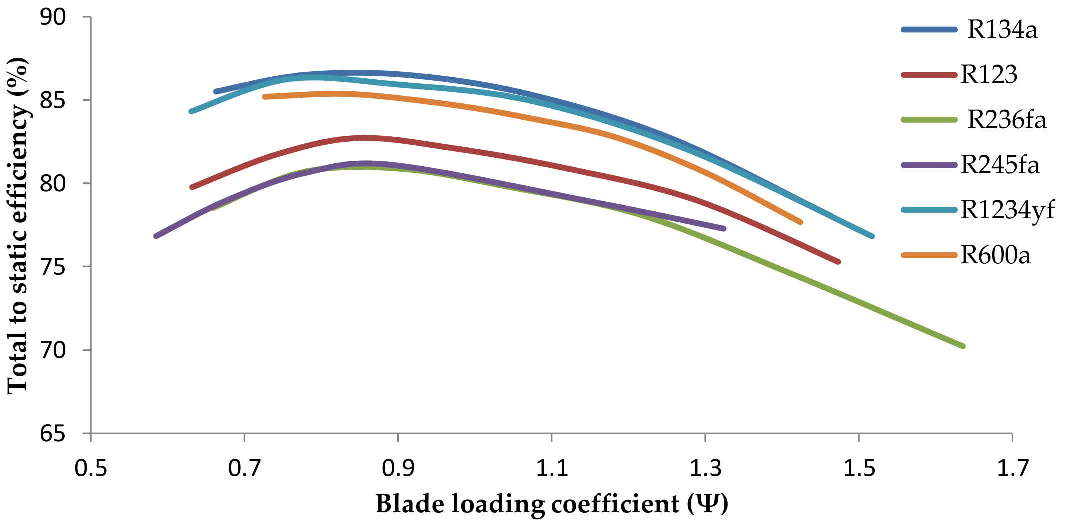

Figure 16. Blade loading coefficients for the selected working fluids with total-to-static efficiency.

A key factor for determining turbine efficiency is the difference between the blade angle and the flow angle (β_2) at the rotor blade leading edge, termed as the incidence angle. As the rotor vanes in radial inflow turbines are assumed to be radial, the angle β_2 is an angle of incidence. Japikse and Baines [30] concluded that peak efficiency for a radial flow turbine is achieved with a negative incidence angle between $-20°$ and $-30°$.

The calculated velocity triangles at the inlet of the rotor presented in Figure 17 indicate that Refrigerants R600a, R123, R236fa, and R245fa have a negative incidence angle away from the recommended range of $-30°$, while R134a and R1234yf are within the range. This leads to a flow separation that can occur on the pressure side of the rotor with a high incidence angle such as the one in R245fa, but this separation cannot be observed for R1234yf, as indicated in Figure 18.

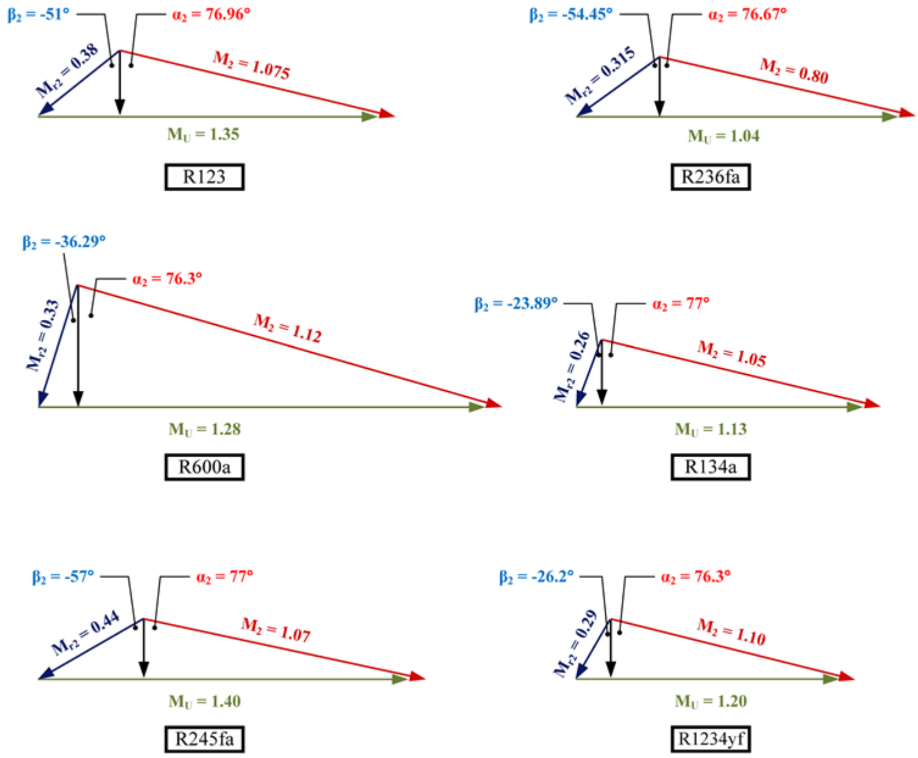

Figure 17. Inlet velocity triangles for the selected working fluids at $U_2/C_0 = 0.7$.

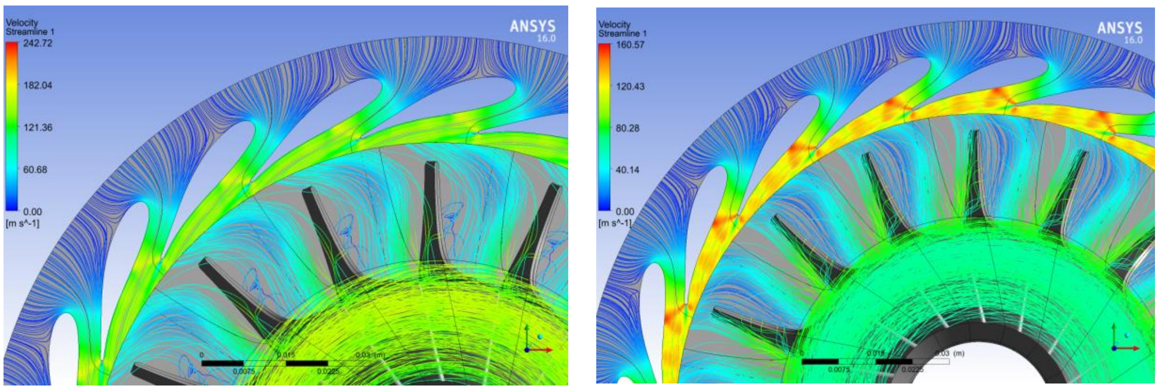

(**a**) (**b**)

Figure 18. 3D velocity streamlines for two working fluids R245fa (**a**) and R1234yf (**b**) at $U_2/C_0 = 0.7$.

4.3. Numerical Results of Zeotropic Mixtures Working Fluids (R600a/R245fa)

The properties of zeotropic mixtures between R245fa and R600a with variable compositions were estimated by using the commercial package REFPROP Version 9.0 [29]. Thereafter, the properties were imported in a finite volume solver ANSYS-CFX (version 16.0) to perform 3D simulations in order to examine the performance of the turbine with these mixtures.

It can be seen from Figure 19 that both mixtures with compositions of 40 R600a and 60 R245fa and of 80 R600a and 20 R245fa improve the turbine performance with 1.6% and 1.15%, respectively at $U_2/C_0 = 0.72$ with respect to pure R245fa. However, the mixture of 60 R600a and 40 R245fa increases the efficiency in 1.64% at $U_2/C_0 = 0.75$ with respect to pure R245fa. It can be noticed that the corresponding efficiency curve for this composition becomes more flat at off-design conditions. Consequently, this mixture can be implemented in solar ORC applications due to the fluctuations in solar heat input.

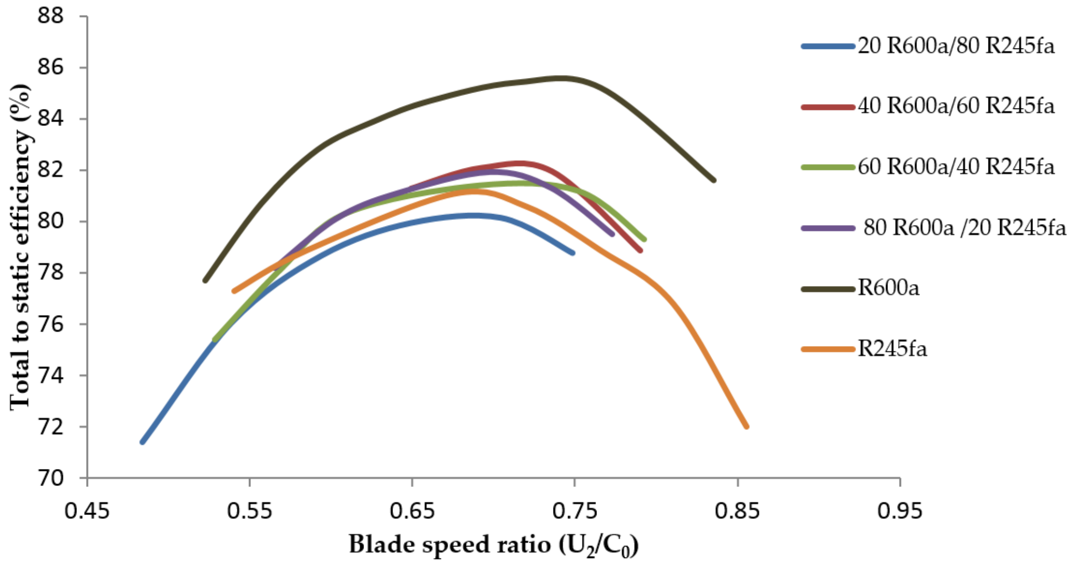

Figure 19. Comparisons of total-to-static efficiency for variable composition zeotropic mixtures (R245fa/R600a) with different blade speed ratios.

5. Conclusions

The current numerical investigation presents the performance of a radial inflow turbo-expander operating within ORC applications. Six pure working fluids (R134a, R600a, R236fa, R245fa, R123, and R1234yf) were investigated for this cycle in order to find the most suitable working fluid. In addition, zeotropic mixtures between R245fa and R600a were examined. The CFD RANS model for the turbo-expander was validated with experimental data from a test rig using air. Switching the turbo-expander from working on air into different working fluids was carried out by selecting the operating conditions that keep the blade speed ratio (U_2/C_0) at 0.7. The steady-state 3D numerical modeling of the turbine at both nominal and off-design conditions was performed in order to get a justification of a radial turbo-expander suitable for low-temperature ORC. The main obtained results are summarized as follows:

- A major issue for the performance of the ORC turbo-expander is the pressure ratio. The best efficiency for the radial inflow turbine was found for R134a and R1234yf as a result of lower pressure ratios across the stage of 2.20 and 2.25, respectively.
- Due to the relatively high GWP of R134a, which has a value of 1430, it should be replaced with R1234yf, which has a low GWP and shows the same turbine performance as R134a.
- At off-design operating conditions, the flow enters the rotor with an incidence angle that is either extremely positive or negative, which leads to an increase in incidence energy loss. Consequently, variable-angle nozzle guide vanes with the control system can be used to maintain the optimum incidence angle at off-design conditions. Therefore, the turbine efficiency can be maintained near the design point.
- A multi-stage radial inflow turbine can be utilized for working fluids (R245fa and R236fa) with high pressure ratios to keep a moderate pressure ratio across a stage.

The findings of the current work are in three areas: (i) switching the gas turbine from air to organic working fluids, (ii) providing a screening of various working fluids in ORC turbo-expanders based on 3D CFD RANS simulations, and (iii) the effect of zeotropic mixtures on the performance of the turbine. Future work will focus on experimental verification of the scaling methodology for a turbo-expander from air to refrigerants.

Acknowledgments: The authors would like to express their thanks to the mechanical engineering department at Ain Shams University for the opportunity to do research at ASU CFD Lab.

Author Contributions: This paper is extracted from a master's thesis prepared by the first author, Ibrahim Gad-el-Hak under the supervision of Nabil A. Mahmoud, Ahmed E. Hussin and Ashraf M. Hamed.

Conflicts of Interest: The authors declare no conflict of interest.

Nomenclature

Symbols

a	sonic velocity ($m \cdot s^{-1}$)
C	absolute velocity ($m \cdot s^{-1}$)
C_0	spouting velocity ($m \cdot s^{-1}$)
h	enthalpy ($J \cdot kg^{-1}$)
M	Mach number ($-$)
N	rotational speed (RPM)
Ω_S	specific speed (rad $(m^3/s)^{0.5}/(J/kg)^{0.75}$)
Q	volume flow rate ($m^3 \cdot s^{-1}$)
p	pressure (MPa)
Pr	pressure ratio (–)
T	temperature (K)
U	blade speed ($m \cdot s^{-1}$)
$y+$	non-dimensional grid spacing at the wall (–)

Greek Letters

α	absolute flow angle (degree)
β	relative flow angle (degree)
η	efficiency (–)
Δ	difference
Φ	flow coefficient (–)
Ψ	blade loading coefficient (–)
ω	angular velocity (rad/s)

Subscripts

0	stagnation value
1	stator inlet station
2	rotor inlet station
3	stage outlet station
c	critical
is	isentropic
s	static
t-s	total-to-static
t-t	total-to-total

Acronyms

ASHRAE	American Society of Heating, Refrigerating, and Air-Conditioning Engineers
ATM	automatic topology meshing
3D	three-dimensional
CFD	computational fluid dynamics
GWP	global warming potential
ORC	Organic Rankine Cycle
ODP	ozone depleting potential
RANS	Reynolds-averaged Navier–Stokes

References

1. Quoilin, S.; Van Den Broek, M.; Declaye, S.; Dewallef, P.; Lemort, V. Techno-economic survey of Organic Rankine Cycle (ORC) systems. *Renew. Sustain. Energy Rev.* **2013**, *22*, 168–186. [CrossRef]
2. Johnson, I.; Choate, W.T.; Davidson, A. *Waste Heat Recovery. Technology and Opportunities in US Industry*; BCS, Inc.: Laurel, MD, USA, 2008.
3. Qiu, G.; Liu, H.; Riffat, S. Expanders for micro-CHP systems with organic Rankine cycle. *Appl. Therm. Eng.* **2011**, *31*, 3301–3307. [CrossRef]

4. Quoilin, S.; Declaye, S.; Legros, A.; Guillaume, L.; Lemort, V. Working fluid selection and operating maps for Organic Rankine Cycle expansion machines. In Proceedings of the 21st International Compressor Conference, Purdue, West Lafayette, IN, USA, 16–19 July 2012; p. 10.
5. Bao, J.; Zhao, L. A review of working fluid and expander selections for organic Rankine cycle. *Renew. Sustain. Energy Rev.* **2013**, *24*, 325–342. [CrossRef]
6. Sauret, E.; Rowlands, A.S. Candidate radial-inflow turbines and high-density working fluids for geothermal power systems. *Energy* **2011**, *36*, 4460–4467. [CrossRef]
7. Lopez Sanz, E. Study on a Radial Turbine Stage with Inlet Guide Vanes for an ORC Process with an Electrical Output of 3.5 kW. Master's Thesis, Universität Stuttgart, Stuttgart, Germany, 2013.
8. Wong, C.S.; Krumdieck, S. Scaling of Gas Turbine From Air to Refrigerants for Organic Rankine Cycle Using Similarity Concept. *J. Eng. Gas Turbines Power* **2016**, *138*, 061701. [CrossRef]
9. Bajaj, S.S.; Patil, H.B.; Kudal, G.B.; Shisode, S.P. Organic Rankine Cycle and Its Working Fluid Selection—A Review. *Int. J. Curr. Eng. Technol.* **2016**, *4*, 20–26.
10. Tchanche, B.F.; Lambrinos, G.; Frangoudakis, A.; Papadakis, G. Low-grade heat conversion into power using organic Rankine cycles—A review of various applications. *Renew. Sustain. Energy Rev.* **2011**, *15*, 3963–3979. [CrossRef]
11. Vélez, F.; Segovia, J.J.; Martín, M.C.; Antolín, G.; Chejne, F.; Quijano, A. A technical, economical and market review of organic Rankine cycles for the conversion of low-grade heat for power generation. *Renew. Sustain. Energy Rev.* **2012**, *16*, 4175–4189. [CrossRef]
12. Schuster, A.; Karellas, S.; Kakaras, E.; Spliethoff, H. Energetic and economic investigation of Organic Rankine Cycle applications. *Appl. Therm. Eng.* **2009**, *29*, 1809–1817. [CrossRef]
13. Gao, H.; Liu, C.; He, C.; Xu, X.; Wu, S.; Li, Y. Performance analysis and working fluid selection of a supercritical organic Rankine cycle for low grade waste heat recovery. *Energies* **2012**, *5*, 3233–3247. [CrossRef]
14. Jumel, S.; Feidt, M.; Kheiri, A. Working fluid selection and performance comparison of subcritical and supercritical organic Rankine cycle (ORC) for low-temperature waste heat recovery. In Proceedings of the ECEEE Summer Study on Energy Efficiency in Industry, Arnhem, The Netherlands, 11–14 September 2012; pp. 559–569.
15. Fiaschi, D.; Manfrida, G.; Maraschiello, F. Thermo-fluid dynamics preliminary design of turbo-expanders for ORC cycles. *Appl. Energy* **2012**, *97*, 601–608. [CrossRef]
16. Aghahosseini, S.; Dincer, I. Exergo-environmental analysis of renewable/waste heat based organic rankine cycle using different working fluid. In Proceedings of the Global Conference on Global Warming, Lisbon, Portugal, 11–14 July 2011.
17. Masheiti, S.; Agnew, B.; Walker, S. An evaluation of R134a and R245fa as the working fluid in an Organic Rankine Cycle energized from a low temperature geothermal energy source. *J. Energy Power Eng.* **2011**, *5*, 392–402.
18. Li, Y.R.; Du, M.T.; Wu, C.M.; Wu, S.Y.; Liu, C. Potential of organic Rankine cycle using zeotropic mixtures as working fluids for waste heat recovery. *Energy* **2014**, *77*, 509–519. [CrossRef]
19. Dixon, S.L.; Hall, C. *Fluid Mechanics and Thermodynamics of Turbomachinery*; Butterworth-Heinemann: Oxford, UK, 2013.
20. Chen, H.; Baines, N.C. The aerodynamic loading of radial and mixed-flow turbines. *Int. J. Mech. Sci.* **1994**, *36*, 63–79. [CrossRef]
21. Cox, G.D. The Practical Design of Turbocharger Turbines Using a Throughflow-Based Optimisation Process. In Proceedings of the ASME Turbo Expo: Turbine Technical Conference and Exposition, Copenhagen, Denmark, 11–15 June 2012; pp. 703–713.
22. Jones, A.C. Design and test of a small, high pressure ratio radial turbine. In Proceedings of the ASME International Gas Turbine and Aeroengine Congress and Exposition, The Hague, The Netherlands, 13–16 June 1994.
23. Sauret, E. Open design of high pressure ratio radial-inflow turbine for academic validation. In Proceedings of the ASME International Mechanical Engineering Congress and Exposition, Houston, TX, USA, 9–15 November 2012; pp. 3183–3197.
24. Siggeirsson, E.M.V.; Gunnarsson, S. Conceptual Design Tool for Radial Turbines. Master's Thesis, Chalmers University of Technology, Gothenburg, Sweden, 2015.

25. Wong, C.S. Design-to-Resource (DTR) Using SMC Turbine Adaptive Strategy: Design Process of Low Temperature Organic Rankine Cycle (LT-ORC). Ph.D. Thesis, University of Canterbury, Christchurch, New Zealand, 2015.
26. Peng, D.Y.; Robinson, D.B. A new two-constant equation of state. *Ind. Eng. Chem. Fundam.* **1976**, *15*, 59–64. [CrossRef]
27. Sauret, E.; Gu, Y. Three-dimensional off-design numerical analysis of an organic Rankine cycle radial-inflow turbine. *Appl. Energy* **2014**, *135*, 202–211. [CrossRef]
28. Hung, T.C. Waste heat recovery of organic Rankine cycle using dry fluids. *Energy Convers. Manag.* **2001**, *42*, 539–553. [CrossRef]
29. *NIST Reference Fluid Thermodynamic and Transport Properties (REFPROP)*, Version 9.0; National Institute of Standards and Technology: Gaithersburg, MD, USA, 2010.
30. Japikse, D.; Baines, N.C. *Introduction to Turbomachinery*; Concepts ETI Inc.: Norwich, UK; Oxford University Press: Oxford, UK, 1997.

© 2017 by the authors. Licensee MDPI, Basel, Switzerland. This article is an open access article distributed under the terms and conditions of the Creative Commons Attribution (CC BY NC ND) license (https://creativecommons.org/licenses/by-nc-nd/4.0/).